AUTONOMOUS NAVIGATION OF MICRO AIR VEHICLE USING ULTRA-WIDEBAND INDOOR POSITIONING IN PRECISION AGRICULTURE

CHING POH LING

SCHOOL OF AEROSPACE ENGINEERING
UNIVERSITI SAINS MALAYSIA

2021

AUTONOMOUS NAVIGATION OF MICRO AIR VEHICLE USING ULTRA-WIDEBAND INDOOR POSITIONING IN PRECISION AGRICULTURE

by

CHING POH LING

Thesis submitted in fulfilment of the requirements for the Bachelor Degree of Engineering (Honours) (Aerospace Engineering)

June 2021

ENDORSEMENT

I, Ching Poh Ling, hereby declare that all corrections and comments made by the supervisor and examiner have been taken consideration and rectified accordingly.

(Signature of Student)

Date: 5 July 2021

(Signature of Supervisor)

Name: Dr Ho Hann Woei

Date: 9/7/2021

DR. HO HANN WOEI
Pensyarah
Pusat Pengajian Kejuruteraan Aeroangkasa
Kampus Kejuruteraan
Universiti Sains Malaysia
14300 Nibong Tebal, Penang
Tel: +604 599 5870 Fax: +604 599 6911

(Signature of Examiner)

Name: Assoc. Prof. Dr. Elmi Abu Bakar

Date: 9/07/2021

Assoc. Prof. Dr. ELMI BIN ABU BAKAR
Lecturer & Researcher
Room 1.26, School of Aerospace Engineering,
Engineering Campus, Universiti Sains Malaysia,
14300 Nibong Tebal, Penang
Tel : +604-599 5954 / 5938 Fax : +604 599 6911

DECLARATION

This thesis is the result of my own investigation, except where otherwise stated and has not previously been accepted in substance for any degree and is not being concurrently submitted in candidature for any other degree.

(Signature of Student)

Date: 5 July 2021

ACKNOWLEDGEMENT

First and foremost, I would like to express my deep and sincere gratitude to my final year project supervisor, Dr Ho Hann Woei, for giving me the opportunity to do this research and providing invaluable guidance throughout the project. His dynamism, vision, sincerity and motivation have deeply inspired me. It was a great privilege and honour to work and study under his guidance. I am incredibly grateful for what he has offered me.

I would also like to extend my thanks to Mr Amir and Mr Zihad, the laboratory technicians, for their help in offering me the resources required in this research. Never forget the moral support and precious advice from these lovely people during my time working on the project.

Furthermore, I am extremely grateful to my friends for their constant motivation and encouragement. Finally, I wish to thank my parents for their love, prayers, caring, and sacrifices to educate and prepare me for my future. I was not able to complete the research without these great people.

AUTONOMOUS NAVIGATION OF MIRCO AIR VEHICLE USING ULTRA-WIDEBAND INDOOR POSITIONING IN PRECISION AGRICULTURE

ABSTRACT

Micro air vehicles (MAVs) have penetrated precision agriculture domains over the past years due to their flexibility and capacity. However, the problem arises when moving the MAV applications into greenhouses, which limits the use of Global Positioning System (GPS). Visual methods have been recently utilized, but the sensors present limitations in greenhouses with the high amount of mist. The challenges remain in position accuracy and robustness in long-term autonomy. To this end, this project proposed a novel system to allow autonomous indoor navigation of MAV using ultra-wideband (UWB) technology. A UWB mobile tag is mounted on the MAV, which actively sending ranging request to a constellation of fixed-position anchors. The MAV is able to self-localize based on the distance measurements fused by an extended Kalman filter (EKF). The position estimation is fed into the control loop to aid the MAV navigation. Various flight tests were carried out successfully in different indoor environments. The results showed that the satisfactory performance of UWB autonomous navigation in greenhouses. The proposed system is expected to reduce labour-intensive activities and possible human error.

NAVIGASI BERAUTONOMI PESAWAT UDARA MIKRO DENGAN TEKNOLOGI JALUR LEBAR ULTRA DALAM PERTANIAN JITU

ABSTRAK

Kebelakangan ini, pesawat udara mikro telah digunakan secara meluas dalam bidang pertanian jitu. Walau bagaimanapun, masalah menimbul apabila mengaplikasikan pesawat udara mikro ke rumah hijau. Hal ini kerana penggunaan sistem kedudukan sejagat dibatalkan di kawasan dalaman. Selain itu, kabut dalam rumah hijau mengehadkan kaedah visual dalam navigasi. Ketepatan kedudukan merupakan satu cabaran dalam autonomi jangka panjang. Dengan itu, kajian ini mencadangkan navigasi pesawat udara mikro dengan meggunakan teknologi jalur lebar ultra. Satu tag mudah alih dipasangkan di pesawat udara mikro. Tag itu akan mengetahui lokasi sendiri dengan mengirakan jarak dengan tag-tag lain yang mempunyai kedudukan tetap. Extended Kalman filter (EKF) akan digunakan untuk menyatukan jarak tersebut dan memasukkan dalam kawalan gelung tertutup untuk membantukan navigasi pesawat udara mikro. Pelbagai ujian penerbangan berjaya dijalankan di persekitaran dalaman yang berbeza. Hasil kajian menunjukkan bahawa prestasi jalur lebar ultra dalam navigasi berautonomi amat memuaskan di rumah hijau. Cadangan ini diharapkan dapat mengurangkan aktiviti intensif buruh dan kemungkinan kesalahan manusia.

TABLE OF CONTENTS

LIST OF FIGURES

LIST OF TABLES

LIST OF ABBREVIATIONS

DCM	Direction Cosine Matrix
DOF	Degree of freedom
DS-TWR	Double sided-two way ranging
EKF	Extended Kalman filter
ESC	Electronic speed controller
FOV	Field of view
GCS	Ground control station
GDOP	Geometric dilution of precision
GNSS	Global Navigation Satellite System
GPS	Global Positioning System
IMU	Inertial measurement unit
INS	Inertial navigation system
IR	Infrared
LiDAR	Light Detection and Ranging
LOS	Line-of-sight
MAV	Micro air vehicle
MCU	ON-chip microprocessor
MOCAP	Motion capture
NHTSA	National Highway Traffic Safety Adminstration
ORB-SLAM	Oriented fast and Rotated Brief SLAM
PID	Proportional-Integral-Derivative
PWM	Pulse-width modulation
QR	Quick response
RF	Radio frequency
RFID	Radio frequency identification
RSS	Signal Strength
RTK	Real-Time Kinematic
SfM	Structure from Motion
SLAM	Simultaneous location and mapping
UGVs	Unmanned ground vehicles
UWB	Ultra-wideband

LIST OF SYMBOLS

x^b, y^b, z^b	:	MAV body reference frame
x^n, y^n, z^n	:	MAV navigation frame
$x^{UWB}, y^{UWB}, z^{UWB}$	:	Local UWB cartesian frame
β	:	Rotated yaw angle [deg]
t_{of}	:	Time of flight [s]
t_{sp}	:	Transmitting time of the poll [s]
t_{rp}	:	Receiving time of the poll [s]
t_{sr}	:	Transmitting time of the response [s]
t_{rr}	:	Receiving time of the response [s]
c	:	Speed of light [m/s]
d	:	Distance
p	:	Position of MAV
v	:	Velocity of MAV
Δt_k	:	Time difference between the last update and the current update
w_k	:	Gaussian white noise with its covariance
$\hat{x}_k^-$	:	Priori state estimation
$\hat{x}_k$	:	Posteriori state estimation
P_k	:	State covariance matrix
Q_k	:	System noise (w) covariance matrix
p^a	:	Distance from an anchor
v_k	:	Zero-mean Gaussian noise
H_k	:	Design matrix
K_k	:	Kalman gain

R_k	:	Covariance matrix of the measurement
I	:	Identity matrix
ϕ	:	Roll [deg]
θ	:	Pitch [deg]
ψ	:	Yaw [deg]
d_{ij}	:	UWB ranging measurement
F	:	Thrust [N]
M_ϕ	:	Rolling moment
M_θ	:	Pitching moment
M_ψ	:	Yawing moment
U	:	Control action
e	:	Error
K_p	:	Proportional gain in control
K_i	:	Integral gain in control
K_d	:	Derivative gain in control

CHAPTER 1

INTRODUCTION

Agriculture commodities provide a source of food for people and animals across the globe. According to Walthall *et al.* (2013), the production of these commodities is vulnerable to climate change, which addresses food security concerns. Greenhouse cultivation is one of the comprehensive systems dealing with such problems, which allows the increase of crop yield (Biek, Chung and Mehta, 2015). A greenhouse is generally a sheltered structure covered by a transparent or partially transparent material for hastening the growth of plants. This kind of agricultural technique is massively utilized for the intensive production of horticultural products in regions with adverse natural climatic conditions since it provides more effective use of daylight and water.

The favourable atmosphere for plant growth attracts pests to thrive as well, making necessary the use of pesticides or continuous monitoring system inside greenhouses. A recent survey reported that about 3 million labourers are affected by poisoning from pesticides every year (Kurkute, 2018). In addition, farmers need to hire many labourers or install cameras or sensors throughout the greenhouses to monitor the crops, which involves a huge amount of investment and effort.

Hence, there is an acute need for robotic solutions in greenhouse automation. One of the well-known projects is AURORA (Mandow *et al.*, 1996), which suggests a robust and low-cost robot autonomously navigates in the greenhouse. Another project for greenhouse automation is AGROBOT (Buemi *et al.*, 1996), a mobile robot with a stereoscopic vision system and a six degree of freedom arm for the greenhouse cultivation of tomatoes. Nevertheless, these unmanned ground vehicles (UGVs) become less agile when moving in narrow rows and irregular ground with the obstacles such as

pipes and hoses inside a greenhouse. They also encounter sinking into soft ground, particularly in the high humidity conditions (Acaccia *et al.*, 2003).

In recent years, there have been a surge of micro air vehicle (MAV) applications in precision agriculture (Zhang and Kovacs, 2012, Mogili and Deepak, 2018) to greatly resolve such UGVs challenges. As the logical heir of UGVs, MAVs have the aerial maneuverability to avoid obstacles inside the greenhouse. At its small size, MAVs are able to access every corner of confined spaces to perform monitoring tasks with its excellent bird's-eye view (Norasma *et al.*, 2019).

MAVs can assist in many tasks in precision agriculture, such as crop monitoring (Bendig, Bolten and Bareth, 2012), soil sampling analysis (Demattê *et al.*, 2018), and fruit harvesting (Kushal *et al.*, 2020). It offers a cost-efficient, risk-reduction, and time-saving solution for greenhouse automation. Despite remote control have been developed (Eschmann *et al.*, 2015), skilled pilots are typically required to operate MAV on-site. Autonomous navigation methods of MAVs have been studied to address this drawback.

To the best of the knowledge, there is no clear definition or established concept and theory for the levels of autonomous MAV navigation in the robotics discipline. The six levels of autonomous vehicle navigation by the National Highway Traffic Safety Administration (NHTSA) are used as the reference of autonomous MAV navigation taxonomy (Vagia and Rødseth, 2019). Level 0 autonomy means that the navigation of MAV is entirely manual controlled by pilots. Level 1 MAV is pilot-guided, but with some automation features for specific flight modes, such as hovering and maintaining altitude. If there is no unexpected change in the flying environment, the MAV is partially automated at Level 2 by navigating based on the scheduled flight path. In Level 3, the MAV recognizes the changing flying environments and controls flight modes for navigation. The next level is high automation, which means the MAV can adapt and react

when there is any system anomaly, such as a collision with other objects. In Level 5, the MAV can autonomously navigate in all environments and situations. To date, Level 2 automation of MAV navigation in a greenhouse is the main focus of this study.

Precise localization is at the forefront of the realization of Level 2 autonomous MAV navigation. Usually, most MAV applications rely heavily on Global Positioning System (GPS). The accuracy of standard GPS is meter-level, and it can be boosted to centimeter-level when running as Real-Time Kinematic (RTK) mode with an additional fixed base station. GPS limits in outdoor uses, and its accuracy is susceptible to poor satellite signal due to multipath effects and blockage of line-of-sight (LOS). On the other hand, a high-precision optical tracking system, VICON (Kushleyev, Mellinger and Kumar, 2013) provides centimeter-level accuracy in an indoor environment, but it requires an expensive and complex setup with multiple cameras.

There are more and more attempts to develop alternatives indoor localization solutions for autonomous MAV navigation without GPS and an expensive VICON system. The outstanding precision and reliability of Light Detection and Ranging (LiDAR) make it widely utilized, but it is not fit for low-cost greenhouse applications. Furthermore, its laser signals are subject to specular reflection, thus it cannot work well in the greenhouse with glass or transparent materials (Shi and Mi, 2020). Another approach is using visual-inertial odometry with either monocular cameras or multiple sensors. However, these sensors present limitations due to the low visibility of dust, smoke, or water inside the greenhouse (Queralta *et al.*, 2020).

In this direction, ultra-wideband (UWB) wireless localization technology has gained increasing attention in MAV applications in the past few years. UWB is a mature radio frequency (RF) technology that has been studied for over two decades (Hellner, 2000), with the IEEE 802.15.4 standard. In contrast with other RF systems, UWB pulses

can be transmitted at frequencies ranging between 3 to 5 GHz and have an RF bandwidth of 1.4 GHz. With the large bandwidth, UWB technology has the properties of strong multipath resistance and, to some extent, wall- penetration. It also avoids the UWB signal from interference with other RF signals, such as remote control and WiFi signals (Guo *et al.*, 2016). With centimeter-level ranging accuracy, small size, and lightweight, the low-power UWB modules can be applied in MAV localization.

In this research, a UWB localization system is proposed for autonomous MAV navigation in greenhouses. The system has an architecture similar to GPS (refer to Figure 1.1), whereby a set of fixed-position anchors transmit signals that are received by the mobile tag within the space. The MAV is able to self-localize based on the distance measurements fused by an extended Kalman filter (EKF). Moreover, an estimated position will be fed into the MAV navigation control unit to aid the navigation.

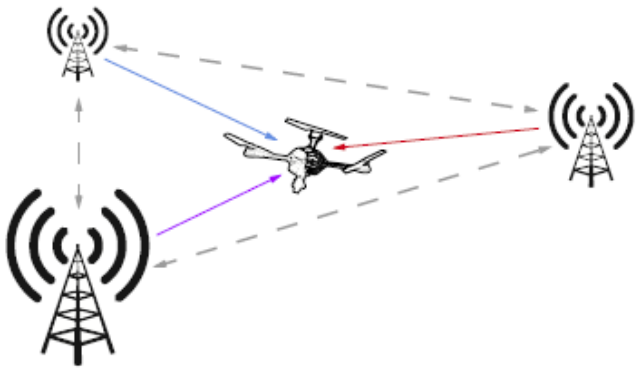

Figure 1.1: The architecture of the UWB localization system (Ledergerber, Hamer and D'Andrea, 2015).

1.1 Problem Statement

According to Riemer and Bechar (2016), labour contributes about 40% of the operational cost in greenhouses for labour-intensive activities such as planting, fertilizing, monitoring, pest control, and harvesting. The enormous force required for the various operations causes bottlenecks that downgrade the productivity of crops and largely open to human error.

Moreover, achievement of the desired conditions in greenhouses often requires the use of pesticides, fungicides, high temperatures, and increased carbon dioxide and humidity levels. Prolonged exposure of greenhouse labourers to these conditions leads to an uncomfortable and hazardous working environment that violates occupational, health, and safety principle (Sammons, Furukawa and Bulgin, 2005).

As mentioned, these manual processes are far outweighed by the economic and social benefits of an autonomous robot. Whilst the development of UGVs has commercial expectations, their dexterity remains a major concern in greenhouse operations as greenhouses only leave very narrow space for service assistants (Acaccia *et al.*, 2003). The inappropriate design of robot locomotion mobility will fail their mission or navigation. Also, their designs are inflexible in different kinds of greenhouse layouts. Other issues to be highlighted are maintenance cost as well as the sizes which are unaffordable for small-scale greenhouse farmers.

Although the MAV application in greenhouses is generally safer and flexible, precise localization is still critical in achieving autonomous navigation. GPS is denied in the greenhouse due to signal degradation until it can no longer support autonomous flight. With the use of LiDAR or the visual odometry method, the challenges remain in position accuracy and robustness in long-term autonomy. While efforts are being put in solving these problems, for instance adding payloads, such as sensors or multi-cameras, the flight endurance and range of MAV (Lee, Ho and Zhou, 2021) will be the constraint to operate inside greenhouses.

Lastly, the presence of external factors in the real-world applications might render the practicability of UWB. The wall or shelves inside greenhouses can interfere with the radiation pattern of UWB signals. Consequently, the accuracy and coverage area of UWB

are potentially affected. Thus, this is a challenge to overcome in UWB-based autonomous navigation.

1.2 Objective

The research work in this thesis is performed to achieve the following objectives:

1. To investigate the feasibility of UWB to achieve cm-level ranging error in indoor environments.
2. To study the effect of different controllers on MAV behaviour in different flight modes.
3. To develop an autonomous MAV to aid greenhouse farmers in precision agriculture.

1.3 Thesis Layout

The five main chapters of this thesis are outlined as follows: Introduction, Literature Review, Methodology, Result and Discussion, Conclusion, and Recommendation. Each chapter is further divided into several sub-chapters as appropriate.

Chapter 1 focuses on the current greenhouse environment with its automation. The problem statement and objectives of the study are introduced in this chapter. Chapter 2 reviews the existing localization methods on MAV autonomous navigation. In Chapter 3, the hardware configuration of MAV and the relevant algorithms are proposed. Chapter 4 covers the results of autonomous navigation based on UWB localization in an indoor environment. Finally, the findings of the work are concluded as well as the recommendations for future works are done in Chapter 5.

CHAPTER 2

LITERATURE REVIEW

It is not a trivial task to localize a MAV in an arbitrary environment. There are several approaches available to address this problem, each with advantages and disadvantages. Generally, the positioning techniques can be separated into two large groups: global and local positioning systems. Global Navigation Satellite System (GNSS) is the standard generic term for satellite navigation systems that provide autonomous geospatial positioning with global coverage, while local positioning systems obtain the position or location information of MAVs in relation to a local field or area.

GPS is the common GNSS system, which is extensively utilized for MAV outdoor navigation. The first GPS named NAVSTAR has been developed in 1978, and its portion ability is reachable to the civil community in 1984. Many MAVs perform outdoor navigation based on GPS since available commercial products already offer a mature performance, such as the mass-produced models from DJI [1]. The accuracy of standard GPS is meter-level. However, for the MAV relies solely on GPS for navigation such an event can be catastrophic, especially in GPS-denied environments. The signals are attenuated by the blockage of line-of-sight (LOS) to the satellite, far-field multipath, or signal diffraction, resulting in MAVs unable to navigate in indoor environments or confined spaces.

GNSS has significant advantages in terms of simplicity and convenience. However, the accuracy of GNSS location measurement is insufficient to expand its usage due to some environmental and systemic factors. It firmly restricts the opportunity of the delicate MAV applications. Numerous studies on correcting the GNSS error are

[1] http://www.dji.com/products/drones

underway to obtain an accurate global location. Real-Time Kinematic GPS (RTK-GPS) is one of the most commonly used and accurate techniques among the studies (Um *et al.*, 2020). Its accuracy can be boosted to centimeter-level with one or more static ground-based reference stations with a known position. One of the RTK-GPS MAV applications in agriculture sectors is Poladrone Oryctes [2], which provides a fast and consistent spraying pesticides workflow without manpower. The big drawback is the cost of this system which makes it unsuitable for this study.

Local (or indoor) positioning system remains novel in the MAVs navigation field. Infrared, radio-frequency, cameras are all different technologies used for the indoor positioning system. A compromise between the approximate accuracy, coverage area, costs, and weight should be taken into account when implementing the system in MAV navigation. Moreover, it has to deal with additional inconveniences, such as the velocity of the MAV, weight and stability problem, limited computation of onboard processor, or air turbulences and acoustic noise caused by the motor in case of using acoustic technology. Balamurugan, Valarmathi and Naidu (2017) provides a useful comparison table on the most promising technological approaches for MAV indoor localization. The extended work by Pérez *et al.* (2019) reviews the main characteristics of the technologies that are most employed in MAV localization. Figure 2.1 (a) shows only 33 results obtained from IEEE Xplore when the search is focused on MAV indoor positioning, while in Figure 2.1 (b), there are approximately 400 works that appear when the search considers 3D indoor positioning, including personal and robot navigation applications.

[2] https://www.poladrone.com/oryctes.html

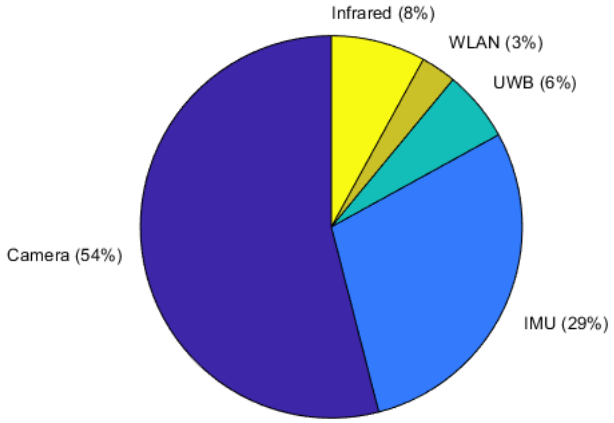

(a) Main technologies for 3D MAV indoor positioning

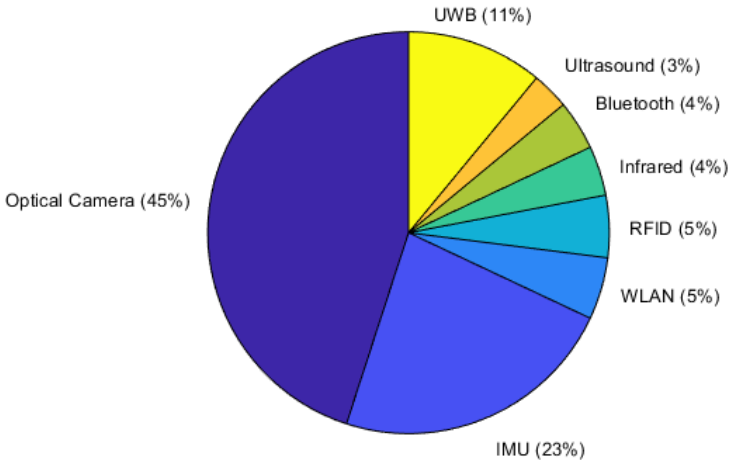

(b) Main technologies for 3D indoor positioning

Figure 2.1: Overview of technology trends in the field of indoor positioning in IEEE Xplore Digital Library (Pérez *et al.*, 2019).

Generally, indoor localization techniques can be divided into three major categories: vision-based, inertial navigation system (INS), and wave characteristics and propagation. More than half of the 3D MAV indoor positioning is based on an optical camera. The use of the Structure from Motion (SfM) is highly concentrated by vision researchers. This approach determines the spatial and geometric relationship of the target through a moving camera, which is a common method of 3D reconstruction. Radwan, Kryjak and Gorgon (2018) succeeded an embedded vision system for SfM computation

in MAV application, which is generally low-cost and hardware simplification. However, the involvement of huge computation makes it less demand in real-time localization.

Simultaneous localization and mapping (SLAM) has been a hot topic in indoor localization. The advancement in SLAM helps the MAV to construct a live map of the surrounding environment while the camera is moving and at the same time localize the MAV using the built map. Monocular SLAM demonstrates good results at short-term localization and even long trajectories (Davison *et al.*, 2007, Weiss, Scaramuzza and Siegwart, 2011) with the fusion of inertial measurement. However, the scale of the map and estimated trajectory is unknown as the depth cannot be measured by using a single camera. Mur-Artal and Tardos (2017) proposed a reliable and lightweight Oriented fast and Rotated Brief SLAM (ORB-SLAM) system for monocular, stereo, and RGB-D cameras, including loop closing, re-localization, and map reuse. Although some recent works presented good performance of SLAM under fast motion (Bloesch *et al.*, 2015), it usually fails at high-speed MAVs in unknown scenarios.

On the other hand, optical flow (Ho, de Croon and Chu, 2017) is a bio-inspired approach that can be defined as the apparent motion of objects, feature points, observed from the eye or the camera. It is frequently used by birds and insects for short-range navigation as well as obstacle avoidance. An optical flow quadrotor helicopter is developed with a 190° field-of-view (FOV) fisheye camera pointing downward. The system uses camera images as primary sensor data for indoor corridor navigation (Zingg *et al.*, 2015). Nevertheless, the challenges such as different terrain and light conditions (Chao, Gu and Napolitano, 2014) need to be addressed for the real greenhouse application.

In recent years, excellent results in this endeavor have been achieved using the motion capture (MOCAP) system, VICON. VICON is a system of high-resolution,

external cameras that can track the six degrees of freedom (DOF) pose of one or more vehicles with sub-millimeter accuracy (How *et al.*, 2008). It is very efficient and robust and usually appears as the ground truth reference to evaluate other approaches. However, it is not appropriate for large greenhouses due to the high cost of installing external cameras. One thing worth pointing out is the difference between onboard and external (offboard) cameras. The MAV is considered autonomous only in the case of onboard cameras (Weiss, Scaramuzza and Siegwart, 2011).

Visual fiducial markers, such as ARTag (Fiala, 2004), AprilTag (Wang and Olson, 2016, Nahangi *et al.*, 2018), and CalTag (Atcheson, Heide and Heidrich, 2010) are the artificial landmarks consisting of patterns. They are designed to be easily recognized and distinguished from one another when they are placed indoors. Unlike quick response (QR) codes, AprilTag markers contain a small information payload, and therefore they can be quickly detected and localized even in different lighting conditions. It is an alternative in a small indoor environment but not ideal for greenhouse applications since its coverage area is less than 10 m.

There are 29 % of the total papers found uses INS as the primary technology. The MAV navigates based on the position, velocity, and orientation estimation from the Inertial Measurement Unit (IMU) which consists of accelerometers, gyroscopes, and magnetometer. The main problem is that it accumulates the position and angular deviation over the travelled distances (Pérez *et al.*, 2019). Thus, INS and vision-based technology often fused with a Kalman filter, which was found to be more accurate. Visual-inertial odometry (Kneip, Chli and Siegwart, 2011, Qin, Li and Shen, 2018) is popular due to its low price and flexibility, but it still presents limitations in low-light or low-visibility conditions. Such a problem is not suitable for greenhouse applications since greenhouses require a high level of mist to maintain an adequate atmosphere. Long-

term autonomy continues to pose challenges in terms of position accuracy and robustness.

The Light Detection and Ranging (LiDAR) is a well-known ranging measurement device. Wallace *et al.* (2012) delivered an example of a UAV-LiDAR system with application to forest inventory. However, the drawback of such platforms is that the size and budget are significantly larger than what could be considered useful as an operational tool in greenhouses. If a single-line LiDAR is applied to MAVs, it can be lighter but only obtain the 2D position of MAV. Another disadvantage is its laser signals cannot function well in a greenhouse with glass or transparent materials (Shi and Mi, 2020).

Moreover, MAV indoor positioning includes the use of infrared (IR). The position of the MAV is determined by incorporating a lightweight IR transmitter into the MAV and using three directional active sensors that receive these signals from the MAV (Kirchner and Furukawa, 2005). This technology is characterized by the absence of radio electromagnetic interference and the power of transmitted IR signal can be easily adjusted to cover only the area of interest. Typical accuracy can vary from centimeter (artificial IR light sources) to meters (in active beacons or when natural radiation is used) (Mautz, 2012). It has drawbacks such as LOS requirements, reflectivity, scattering, and can be adversely affected by sunlight.

Radio-based localization systems, such as Radio Frequency Identification (RFID), WiFi, Bluetooth, Zigbee, and ultra-wideband (UWB), are emerging technologies in indoor positioning. The RFID technology works without direct LOS since the radio waves have the ability to penetrate solid materials, but the strength of signals depends upon the density of objects in the building, and hence its accuracy is affected. In Song *et al.* (2006), the researcher used RFID tags for automating the tasks of

tracking the delivery of materials on construction sites. The main concern of using RFID technology in greenhouse application is the limited coverage range.

WiFi and Zigbee are both configured as wireless network systems. By the calculated distance based on Signal Strength (RSS) values, the position can be obtained. WiFi is relatively cheap and low invasive. However, to date, there is no successful MAV flight using WiFi localization has been reported. This can be attributed to its unsatisfactory accuracy (Nguyen *et al.*, 2016). Whereas Zigbee improves the positioning accuracy, but it is still difficult to maintain a collision-free MAV formation in limited indoor space (Li *et al.*, 2018).

In contrast to the researches discussed above, the UWB localization system presented in this work has a promising solution in terms of accuracy, coverage range, and development cost. The miniature of a single chip transceiver eliminates the weight and stability problem, consequently increases the overall flight endurance and range of MAV when operating in greenhouses. With the large bandwidth, UWB technology has the properties of strong multipath resistance and the ability to pass through obstacles. At the same time, its high capacity data transmission with low energy consumption can be implemented in real-time localization. With its centimeter-level ranging error, the MAV is able to spray pesticides without waste or monitor the crops precisely. The system is expected to operate efficiently in greenhouses.

CHAPTER 3

METHODOLOGY

This study focuses on the localization and navigation of MAV in GPS-denied environments based on UWB technology. The UWB module on the moving MAV is to actively send ranging requests to UWB anchors at known positions to obtain the distance measurements. Once a range measurement is retrieved, it will be fused by the extended Kalman filter (EKF) for position estimation. Moreover, an estimated position will be fed into the flight control unit for MAV navigation. Various autonomous flight tests have been conducted with a QAV250 quadrotor equipped with a Pixhawk running with Ardupilot firmware.

3.1 System Overview

An overview of the hardware configuration is shown in Figure 3.1. The components are arranged wisely to maintain a good centre of gravity (CG).

A carbon-fiber QAV250 frame is chosen as it is small and low-risk to fly in a confined space. The MAV is radio-controlled by using a Taranis Q-X7 transmitter which communicates with a FrSky 2.4 GHz ACCST X8R receiver. A Holybro telemetry radio with 433 MHz provides a wireless MAVLink connection between the ground control station (GCS) and MAV. It allows for parameter tuning while the MAV is in flight, real-time telemetry inspection, mission changes on the fly, and so on. The three main electronic components that constitute the onboard avionics are the UWB transceiver, Arduino Nano, and Pixhawk Autopilot.

The UWB transceiver in use is DecaWave's DW1000 UWB sensor and STMicroelectronics STM32F103 as the on-chip microprocessor (MCU). The MCU is connected to the DW1000 UWB sensor through the SPI interface. DW1000 is a low-

power, low-cost wireless transceiver chip that complies with IEEE 802.15.4-2011. Within the range of 40 m, it has a high level of positioning accuracy and multipath immunity. Its dimension of $50 \times 60 \times 1$ mm and weight of 20 g are suitable for our MAV.

The Arduino Nano is a small, complete, and breadboard-friendly board based on the ATmega328. It hosts and directs the UWB transceiver to collect the distances to the anchors. Then, it communicates the localization message with Pixhawk for MAV navigation.

The Pixhawk Autopilot has an embedded inertial measurement unit (IMU) composed of an accelerometer, gyroscope, and magnetometer. The Proportional-Integral-Derivative (PID) controller normally uses GPS input for outdoor flight when GPS is reliable. In this study, UWB acts as a fake-GPS input to support the indoor flight, while the altitude is still primarily measured from the barometer. Their update rates are 140 Hz and 100 Hz, respectively.

In the autopilot control system, the feedback controller is capable of controlling the speed of motors through electronic speed controllers (ESCs). All the electronic components are powered by a 3-cell LiPo battery with a capacity of 6000 mAh. The detailed wiring diagram refers to Figure 3.2.

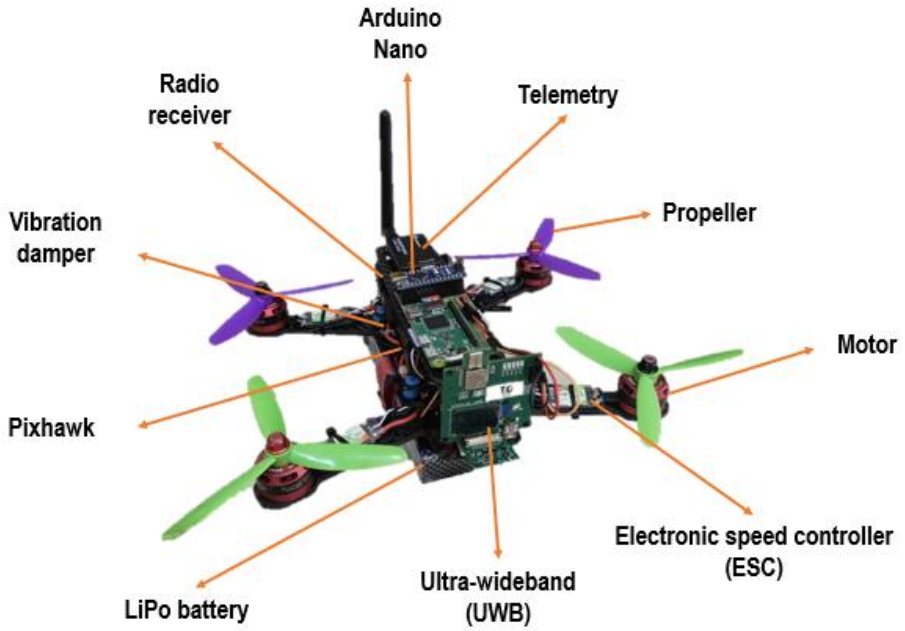

Figure 3.1: An overview of the system hardware configuration.

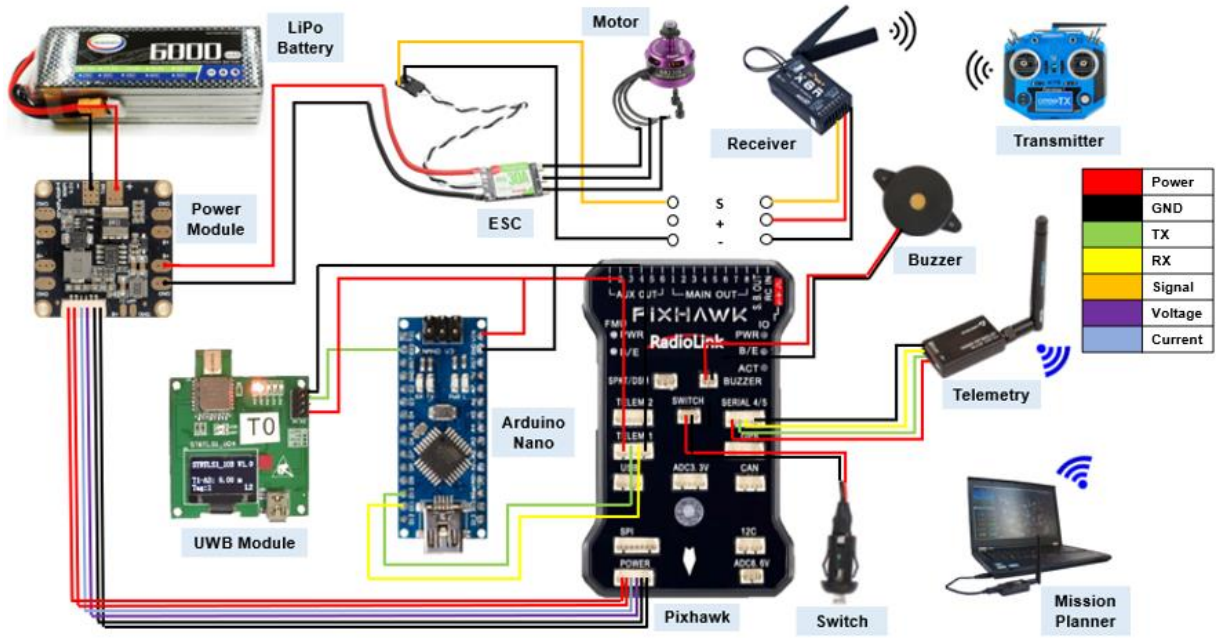

Figure 3.2: Detailed Wiring diagram.

3.2 Coordinate Systems

Figure 3.3 gives an overview of coordinate frames that are relevant for this work. The reference body frame is fixed to the MAV and its x^b-axis is aligned to the MAV longitudinal axis, its z^b-axis is perpendicular to the MAV center plate and intersects with the MAV's center of gravity. The y^b-axis is chosen to be right-handed orthogonal.

The origin of the navigation frame is the position of UWB anchor A0. Its x^n-axis is pointing towards magnetic north, and its z^n-axis in the opposite direction of the Earth's gravitational force. The y^n-axis is again perpendicular to both axes and is directed in such a way that (x^n, y^n, z^n) is a right-handed triad.

The local UWB cartesian frame is constructed based on the position of the UWB anchors. The rules of thumb for the anchor configuration are to place them high where there is a good line of sight with no obstructions between them and to spread the anchors around to obtain a good geometric dilution of precision (GDOP) which suggests a better precision of intersection. To optimal antenna performance, it is advised to orient all the antennas vertically and make sure there are no heavy metal objects placed near the antennas (Decawave, 2016).

The origin and the z-axis of the local UWB cartesian frame and the navigation frame are identical. For simplicity, it is recommended that both frames be set up in the same way as shown in Figure 3.3 (a). Refer to Figure 3.3 (b), in the case that the two frames are rotated against each other about a fixed but unknown angle, the position estimation of the local UWB cartesian frame have to be rotated into the body frame since the MAV's position control relies on the measurements in the body frame. In this approach, the rotated angle is known as yaw angle, β and the equations are presented below:

$$x^b = x^{UWB} \cos\beta - y^{UWB} \sin\beta \tag{3.1}$$

$$y^b = x^{UWB} \sin\beta + y^{UWB} \cos\beta \tag{3.2}$$

$$z^b = z^{UWB} \tag{3.3}$$

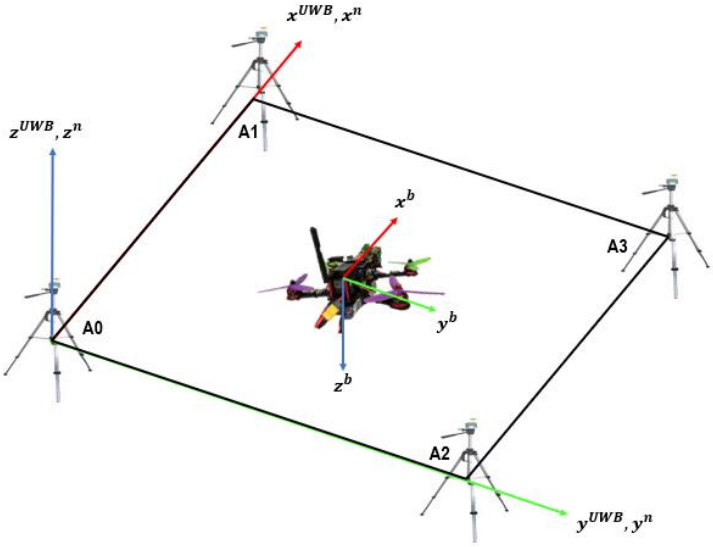

(a) For simplicity, the four UWB anchors (A0, A1, A2, and A3) are constructed identically with the navigation frame.

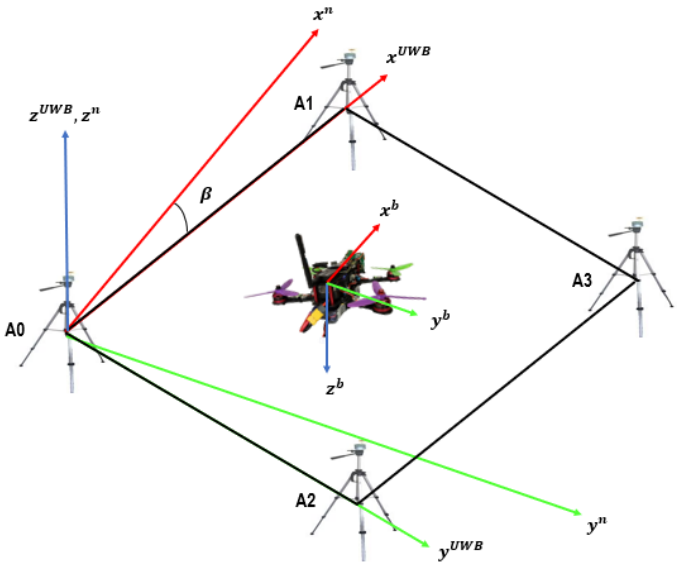

(b) The four UWB anchors (A0, A1, A2, and A3) are constructed with a rotated angle, β with the navigation frame.

Figure 3.3: Important coordinate frames used in this work: the navigation frame (***n***), the local UWB cartesian frame (***UWB***), and the MAV body frame (***b***).

3.3 Double Sided-Two Way Ranging

The distances between MAV-anchor pairs are obtained using Double Sided-Two Way Ranging (DS-TWR) as described in DecaWave's application note [3]. The main advantage of DS-TWR is to compensate for the clock offset between the mobile tag and anchor.

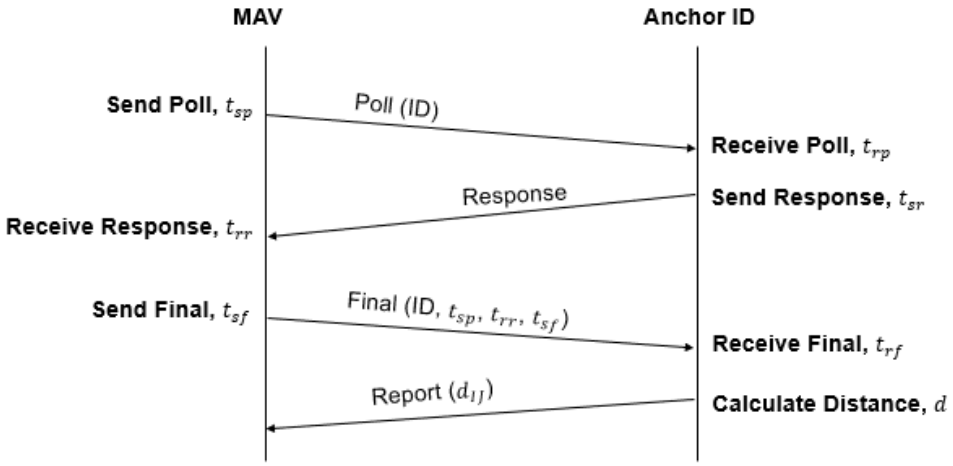

Figure 3.4: Timestamps and communication required for single MAV-anchor pairs (Strohmeier *et al.*, 2018).

Figure 3.4 summarizes the communication flow for a single MAV-anchor pair. A poll message is sent from MAV with a certain ID. An anchor with the correct ID responses to the poll message and consequently the transmitting time, t_{sp} and receiving time, t_{rp} are logged. Again, the transmitting time of the response, t_{sr} as well as the receiving time of the response, t_{rr} are logged on the anchor and the MAV respectively. The time of flight, t_{of} between both nodes can be computed by the following equation:

[3] DecaWave, "Application note:APS016 Moving From TREK1000 to a Product,"pp. 1-22, 2015.

$$t_{of} = \frac{(t_{rr} - t_{sp})(t_{sr} - t_{rr}) - (t_{sr} - t_{rp})(t_{rf} - t_{sr})}{t_{sf} - t_{sp} + t_{rf} - t_{rp}} \quad (3.4)$$

The distance can be calculated by using the speed of light, $c = 3 \times 10^8\ m/s$,

$$d = t_{of} \times c \quad (3.5)$$

The t_{of} ranging reports are logged in the format as follows (DecaWave, 2016):

MID	MASK	RANGE0	RANGE1	RANGE2	RANGE3	NRANGES	RSEQ	DEBUG	aT:A

Example:

mr	0f	000005a4	000004c8	00000436	000003f9	0958	C0	40424042	a0:0

Description:

MID	**Message ID:** **"mr" message consists of the tag to anchor raw ranges,** **"mc" tag to anchor range bias-corrected ranges – used for tag location, and** **"ma" anchor to anchor range bias-corrected ranges – used for anchor auto-positioning.**
MASK	**RANGEs are valid, if MASK=7 then only RANGE0, RANGE1, and RANGE2 are valid (in hex, 8-bit number)**
RANGE0	**Tag to anchor ID 0 range if MID = mc/mr (in mm, 32-bit hex number)**
RANGE1	**Tag to anchor ID 1 range if MID = mc/mr or** **Anchor ID 0 to anchor ID 1 range if MID = ma (in mm, 32-bit hex number)**
RANGE2	**Tag to anchor ID 2 range if MID = mc/mr or** **Anchor ID 0 to anchor ID 2 range if MID = ma (in mm, 32-bit hex number)**
RANGE3	**Tag to anchor ID 3 range if MID = mc/mr or** **Anchor ID 1 to anchor ID 2 range if MID = ma (in mm, 32-bit hex number)**
NRANGES	**Number of ranges completed by reporting unit raw range (16-bit hex number)**
RSEQ	**Range sequence number (8-bit hex number)**
DEBUG	**TX/RX antenna delay (if MID = ma) – two 16-bit numbers or time of last range**
aT:A	**T is tag ID, and A is anchor ID**

Once the distance is calculated, the result is reported back to the MAV, resulting in a total number of four messages per distance measurement.

3.4 Trilateration

Trilateration is a mathematical technique in which the location of a mobile tag can be determined by obtaining simultaneous range measurements from the anchors with known coordinates. With only four noncoplanar UWB anchors, a minimal configuration of anchors will be used that allows a valid 3D position estimation with a low communication load. In Figure 3.5, there are three anchors act as the reference points with coordinates (x_1, y_1, z_1), (x_2, y_2, z_2), and (x_3, y_3, z_3). The mobile tag (x, y, z) is estimated as a central point by intersecting the three spheres. The mobile tag is assumed placed on the intersection point (Thomas and Ros, 2005).

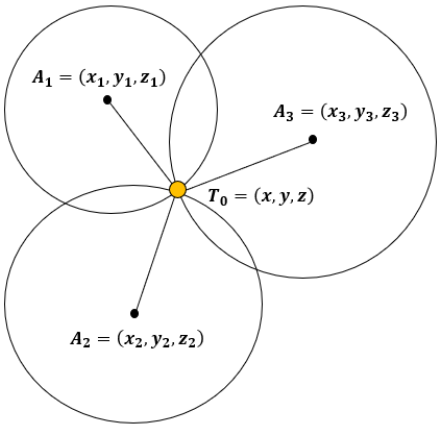

Figure 3.5: Trilateration algorithm illustration

Denote the coordinates of the i-th anchors (x_i, y_i, z_i) and its distance d_i, the solutions to the system of quadratic equations can be obtained from

$$(x - x_i)^2 + (y - y_i)^2 + (z - z_i)^2 = {d_i}^2 \tag{3.6}$$

Each part of Eq. (3.6) will be subtracted with the other part distance which can be obtained to this following equation using matrix formula based on the number of anchors as reference point respectively (Manolakis, 1996):

$$P = (A^T A)^{-1} A^T B \tag{3.7}$$

where P is a column vector $(x, y, z)^T$ representing the calculated coordinates of the tag. Note that all elements in matrix $L = (A^T A)^{-1} A^T$ are derived from reference coordinates only. Moreover, matrix B is a column vector that consists of the distances between the central point and all the reference points.

Assume $i \in [1,2,3 \ldots . n]$, the mobile tag will calculate its position (x, y, z) using trilateration or multi-lateration based on the following formula:

$$P = \begin{bmatrix} x \\ y \\ z \end{bmatrix} \rightarrow A = 2 \begin{bmatrix} (x_{i=1} - x_{i+1}) & (y_{i=1} - y_{i+1}) & (z_{i=1} - z_{i+1}) \\ (x_{i=1} - x_{i+2}) & (y_{i=1} - y_{i+2}) & (z_{i=1} - z_{i+2}) \\ \cdots & \cdots & \cdots \\ (x_{i=1} - x_n) & (y_{i=1} - y_n) & (z_{i=1} - z_n) \end{bmatrix} \quad (3.8)$$

The B matrix component can be computed as below:

$$B = \begin{bmatrix} {d_{i+1}}^2 - {d_{i=1}}^2 - ({x_{i+1}}^2 + {y_{i+1}}^2 + {z_{i+1}}^2) + ({x_{i=1}}^2 + {y_{i=1}}^2 + {z_{i=1}}^2) \\ {d_{i+2}}^2 - {d_{i=1}}^2 - ({x_{i+2}}^2 + {y_{i+2}}^2 + {z_{i+2}}^2) + ({x_{i=1}}^2 + {y_{i=1}}^2 + {z_{i=1}}^2) \\ \cdots \\ {d_n}^2 - {d_{i=1}}^2 - ({x_n}^2 + {y_n}^2 + {z_n}^2) + ({x_{i=1}}^2 + {y_{i=1}}^2 + {z_{i=1}}^2) \end{bmatrix} \quad (3.9)$$

The algorithms for trilateration and multi-lateration in 3D are summarized in Figure 3.6 and Figure 3.7, respectively.

Algorithm 1 Algorithm for Trilateration in 3D

Input: Range of anchors to tag & coordinates of anchors
$\{d_1, d_2, d_3\}$ & $\{(x_1, y_1, z_1), (x_2, y_2, z_2), (x_3, y_3, z_3)\}$

Output: Coordinates of the tag using trilateration
$(x_{123}, y_{123}, z_{123})$

1. Distance: $d_{temp} \leftarrow \sqrt{(x_2 - x_1)^2 + (y_2 - y_1)^2 + (z_2 - z_1)^2}$
2. $d'_{temp} \leftarrow \sqrt{(x_3 - x_1)^2 + (y_3 - y_1)^2 + (z_3 - z_1)^2}$
3. $x' \leftarrow \left(d_1^2 - d_2^2 + d_{temp}^2\right) / \sqrt{2 d_{temp}}$
4. $y' \leftarrow (d_1^2 - d_3^2 + d'^2_{temp} - 2x_3 x') / 2y_3$
5. $z' \leftarrow \sqrt{d_1^2 - x'^2 - y'^2}$
6. $x_{123} \leftarrow x'$
7. $y_{123} \leftarrow y'$
8. $z_{123} \leftarrow z'$

Figure 3.6: Algorithm for Trilateration in 3D.

Algorithm 2 Algorithm for Multi-lateration in 3D

Input: Distance between anchors and tag
$\{d_1, d_2, d_3, d_4\}$ & $\{(x_1, y_1, z_1), (x_2, y_2, z_2), (x_3, y_3, z_3), (x_4, y_4, z_4)\}$

Output: Coordinates of the tag in 3D
(x, y, z)

1. $T_{123}(x_{123}, y_{123}, z_{123}) \leftarrow$
   Trilateration $\{d_1, d_2, d_3\}$ & $\{(x_1, y_1, z_1), (x_2, y_2, z_2), (x_3, y_3, z_3)\}$
2. $T_{124}(x_{124}, y_{124}, z_{124}) \leftarrow$
   Trilateration $\{d_1, d_2, d_4\}$ & $\{(x_1, y_1, z_1), (x_2, y_2, z_2), (x_4, y_4, z_4)\}$
3. $T_{134}(x_{134}, y_{134}, z_{134}) \leftarrow$
   Trilateration $\{d_1, d_3, d_4\}$ & $\{(x_1, y_1, z_1), (x_3, y_3, z_3), (x_4, y_4, z_4)\}$
4. Tag's position $(x, y, z) \leftarrow$
   Centroid $(T_{123}, T_{124}, T_{134})$

Figure 3.7: Algorithm for Multi-lateration in 3D.

3.5 Extended Kalman Filter

A high-level EKF estimation is utilized as the fake-GPS input for the sensor fusion algorithm of the Pixhawk, which is set to use the 22-state EKF attitude and position estimator. In this 22-state EKF, the position, velocity, and attitude states are predicted by the integration of acceleration and angular rate measurements from the IMU. In the correction step, range measurements obtained from UWB are substituted and the relevant noise parameters are adjusted accordingly (Nguyen *et al.*, 2016).

The working principle of the filter is described mathematically as the following. Let $p = \left(p_x\ , p_y\ , p_z\right)'$ be the MAV's position, $v = \dot{p}$ be its velocity, and $w(t)$ is Gaussian white noise. By assuming the acceleration remains constant in $[t_{k-1}, t_k]$, the MAV's motion is modeled as follows:

$$X_k = \begin{bmatrix} p_k \\ v_k \end{bmatrix}; \quad X_{k+1} = A_k X_k + w_k \tag{3.10}$$

where $A_k = \begin{bmatrix} I & \Delta t_k I \\ 0 & I \end{bmatrix}$ is a 6×6 discrete state transition matrix, Δt_k is the time difference between the last update and the current update, and w_k is the Gaussian white noise with its covariance.

Applying the EKF to the system (3.10) yields the localization equations as follows, with $\hat{x}_k^-$ and $\hat{x}_k$ being a priori and a posteriori state estimation at the time t_k.

Process update ("Prediction")

$$\hat{x}_k^- = A_{k-1}\hat{x}_{k-1} \tag{3.11}$$

$$P_k^- = A_{k-1}P_{k-1}A_{k-1}^T + Q_{k-1} \tag{3.12}$$

where P_k is the state covariance matrix, and Q_k is the system noise (w) covariance matrix.

The measurement equation can be found as we assume that the measurement is the distance from an anchor (denoted as p^a) to the MAV's position subject to a zero-mean Gaussian noise ν_k.

$$d_k = \|p_k^- - p^a\| + \nu_k \tag{3.13}$$

Measurement update ("Correction")

$$\hat{d}_k = \|\hat{p}_k^- - p^a\| \tag{3.14}$$

$$H_k = \frac{1}{\hat{d}_k}[(\hat{p}_k^- - p^a)^T \quad 0]_{6\times 1} \tag{3.15}$$

$$K_k = P_k^- H_k^T (H_k P_k^- H_k^T + R_k)^{-1} \tag{3.16}$$

$$\hat{x}_k = \hat{x}_k^- + K_k\left(d_k - \hat{d}_k\right) \tag{3.17}$$

$$P_k = (I - K_k H_k)P_k^- \tag{3.18}$$

where H_k is the design matrix, K_k is the Kalman gain, R_k is the covariance matrix of the measurement, and I is the identity matrix.